ACS OMEGA

Open Access

http://pubs.acs.org/journal/acsodf

Article

First Reusable Catalyst for the Reductive Coupling Reaction of Organohalides with Aldehydes†

Hamed Zarei, Sara Sobhani,* and José Miguel Sansano

Cite This: *ACS Omega* 2023, 8, 36801−36814

Read Online

ACCESS | Metrics & More | Article Recommendations | Supporting Information

ABSTRACT: In this study, we simulate the reductive coupling (Barbier−Grignard-type) reaction of organohalides with aldehydes using a new reusable catalyst. In this regard, bimetallic alloys of NiCo encapsulated in melamine-based dendrimers (MBD) immobilized on magnetic nanoparticles symbolized as γ-Fe_2O_3-MBD/NiCo were designed and synthesized. The structure and properties of the catalyst were studied by a variety of techniques such as Fourier transform infrared (FT-IR) spectroscopy, X-ray diffraction (XRD), X-ray photoelectron spectroscopy (XPS), transmission electron microscopy (TEM), thermogravimetric analysis (TGA), vibrating sample magnetometry (VSM), energy-dispersive spectrometry (EDS) mapping, and inductively coupled plasma (ICP). The presence of NiCo nanoalloys was confirmed by XRD and XPS analysis, TEM images, and EDS mapping. Various secondary alcohols were produced in good to high yields by reductive coupling of different types of aldehydes and organohalides in the presence of HCO_2K as a nonmetallic reducing agent in aqueous media catalyzed by γ-Fe_2O_3-MBD/NiCo. In these reactions, the high catalytic performance of γ-Fe_2O_3-MBD/NiCo was achieved in comparison to monometallic counterparts due to the synergistic cooperative effect of Co and Ni in the NiCo nanoalloys. Magnetic and hydrophilic properties of the catalyst facilitate the catalyst recyclability for seven runs. The reusability of γ-Fe_2O_3-MBD/NiCo, use of water as an environmentally friendly solvent, ease of processing, and absence of metal additives make this process an excellent choice for the reductive coupling reaction to produce secondary alcohols from aldehydes. This is the first report on these kinds of reactions using a reusable catalyst.

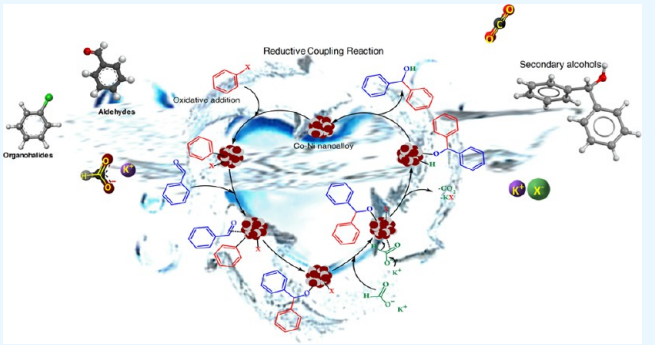

1. INTRODUCTION

The Grignard reaction, nucleophilic addition of organomagnesium reagents to aldehydes for producing secondary alcohols, is an important technique for the C−C bond formation.[1] This method requires (1) stoichiometric amounts of organometallic reagents, for which their synthesis is not easy to manage, (2) temperature control to overcome the exothermic nature of the Grignard reaction, and (3) strict control of anhydrous conditions. Moreover, Grignard reactions suffer from low functional group compatibility due to the basic and nucleophilic properties of organomagnesium reagents. In the Barbier−Grignard-type reaction, as a modified procedure for C−C bond formation, organometallic reagents have been produced by the in situ reaction of aryl halides with metals.[2] Although, this method solved the problem of handling and storage of air-sensitive organometallic reagents by their in situ formation, it still requires stoichiometric amounts of organometallic reagents (Scheme 1a).[3] Catalytic strategies are appealing alternatives.[4] For instance, the Nozaki−Hiyama−Kishi (NHK) reaction is a chromium-mediated protocol for the preparation of secondary alcohols via catalytic carbonyl reductive couplings of organohalides and aldehydes.[5] This method is generally catalyzed by nickel catalysts. Ni catalysts promote organohalides to produce nucleophilic organochromium species through trans-metalation with Cr(III).[6] However, these reactions have a significant disadvantage of the necessity of using a large amount of toxic chromium compounds. Some chromium-free methods using Zn (with stoichiometric amounts), BEt_3, $ZnEt_2$, $AlMe_3$ (pyrophoric compounds), and R_3SiH (expensive/mass-intensive) have been developed.[6,7] Further improvement was achieved by using nonmetallic reductants (H_2, *iso*-propanol) and hydrogen autotransfer reactions.[8] Aside from these reducing agents, sodium formate, which is known as a benign inexpensive low-molecular-weight reductant, has been reported by Kirische for the first time for Rh-catalyzed carbonyl reductive couplings.[4c] However, this method suffers from using an expensive and unreusable catalyst, a toxic organic solvent, and phosphorus ligands, requiring basic

Received: May 16, 2023
Accepted: September 18, 2023
Published: September 29, 2023

Scheme 1. Utilizing Aryl Halides to Access Secondary Alcohols via Barbier−Grignard-Type Arylation of Aldehydes

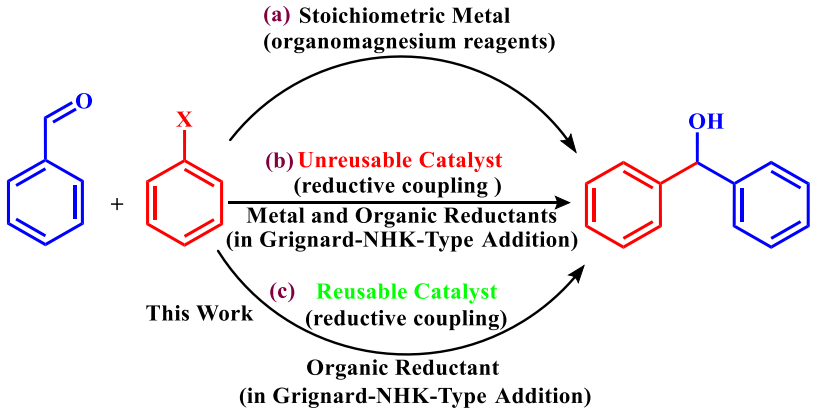

Scheme 2. Reductive Coupling Reaction Using γ-Fe_2O_3@MBD/PdCo as a Catalyst

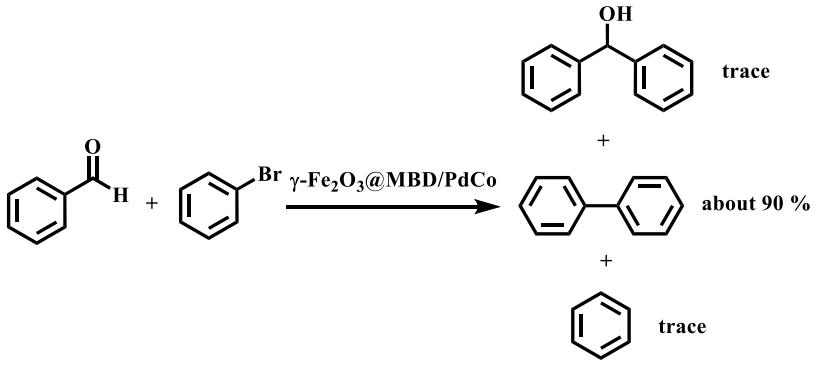

conditions, high temperature (130 °C) and long reaction time (16 h) (Scheme 1b). In this report, we introduce the first reusable catalyst for these kinds of reactions (Scheme 1c).

Using bimetallic nanoalloys as catalysts in organic transformations have been documented as a fascinating approach to improve the catalytic activity of metal-based catalysts.[9] In the bimetallic catalysts, each single metal can exhibit both inherent and new chemical properties.[10] Moreover, synergistic metal interactions in bimetallic catalysts could alter the surface properties of individual metals, stabilize the active species, improve the resistance to poisoning, and reduce the cost.[11]

Among the catalytic metals (Ni,[4ab12] Rh,[4c] Ru,[13] Co,[4f] and Pd,[14] etc.) employed for the reductive reactions, Ni-based catalysts are the most extensively used due to their comparatively high hydrogenation activity.[15] To increase the selectivity and reactivity of Ni-based catalysts, bimetallic nanoalloys are commonly formed by combining Ni with cobalt.[15f16] However, the produced nanoalloys are sensitive to air oxidation. To improve the stability of alloy materials several capping/protecting agents including long chain acids, amines, carbon, phosphine oxides, polymers, dendrimers, and surfactants are often used in their synthetic process.[17]

Dendrimers are highly branched symmetrical polymers, which spread over three dimensions.[18] Their uniform structure makes them as templates for the synthesis of nanoparticles (NPs). The stability of the produced NPs is increased by their encapsulation within the cavities of the dendrimers. Furthermore, the encapsulation of the NPs prevents their agglomeration and makes it possible to synthesize well-dispersed and small size nanoparticles.[19]

In our ongoing attempt to improve a benign catalyzed reaction,[20] recently we have introduced magnetically recyclable Pd−Co bimetallic alloys encapsulated in melamine-based dendrimers (MBD) as a catalyst in the C−C coupling reactions in aqueous media.[17d] Our efforts with this catalyst to produce secondary alcohols from the reductive coupling of aryl halides with aldehydes were unsuccessful. Such reductive couplings overwhelmed side reactions such as reductive homocoupling or a dehalogenation reaction of aryl halides (Scheme 2). Avoiding this side product formation, we sought for a new bimetallic alloy with more selectivity that might be capable of catalyzing the formation of secondary alcohols from the reductive coupling of organohalides with aldehydes. Since nickel is a general and the cheapest catalyst for these kinds of reactions, herein, a bimetallic alloy of NiCo encapsulated in a melamine-based dendrimer immobilized on magnetic nanoparticles (γ-Fe_2O_3@MBD/NiCo) has been synthesized, and its catalytic activity as a nanomagnetically reusable catalyst has been studied in the reductive coupling reaction of organohalides with aldehydes.

2. RESULTS AND DISCUSSION

2.1. Synthesis and Characterization of γ-Fe_2O_3-MBD/NiCo. Scheme 3 shows the approach used to prepare the bimetallic NiCo catalyst (γ-Fe_2O_3@MBD/NiCo). In the first step, γ-Fe_2O_3 was functionalized by reacting with 3-chloropropyltrimethoxysilane, followed by treatment with melamine to yield γ-Fe_2O_3-melamine [Scheme 3, half-generation (G0.5)]. The reaction of γ-Fe_2O_3-melamine with epichlorohydrin (ECH) as a bifunctional molecule for growing dendritic branches [Scheme 3, first generation (G1)] and then the ring opening reaction of the terminal epoxide in γ-Fe_2O_3-melamine-ECH

https://doi.org/10.1021/acsomega.3c03414
ACS Omega 2023, 8, 36801−36814

Scheme 3. Synthesis of γ-Fe_2O_3@MBD/NiCo

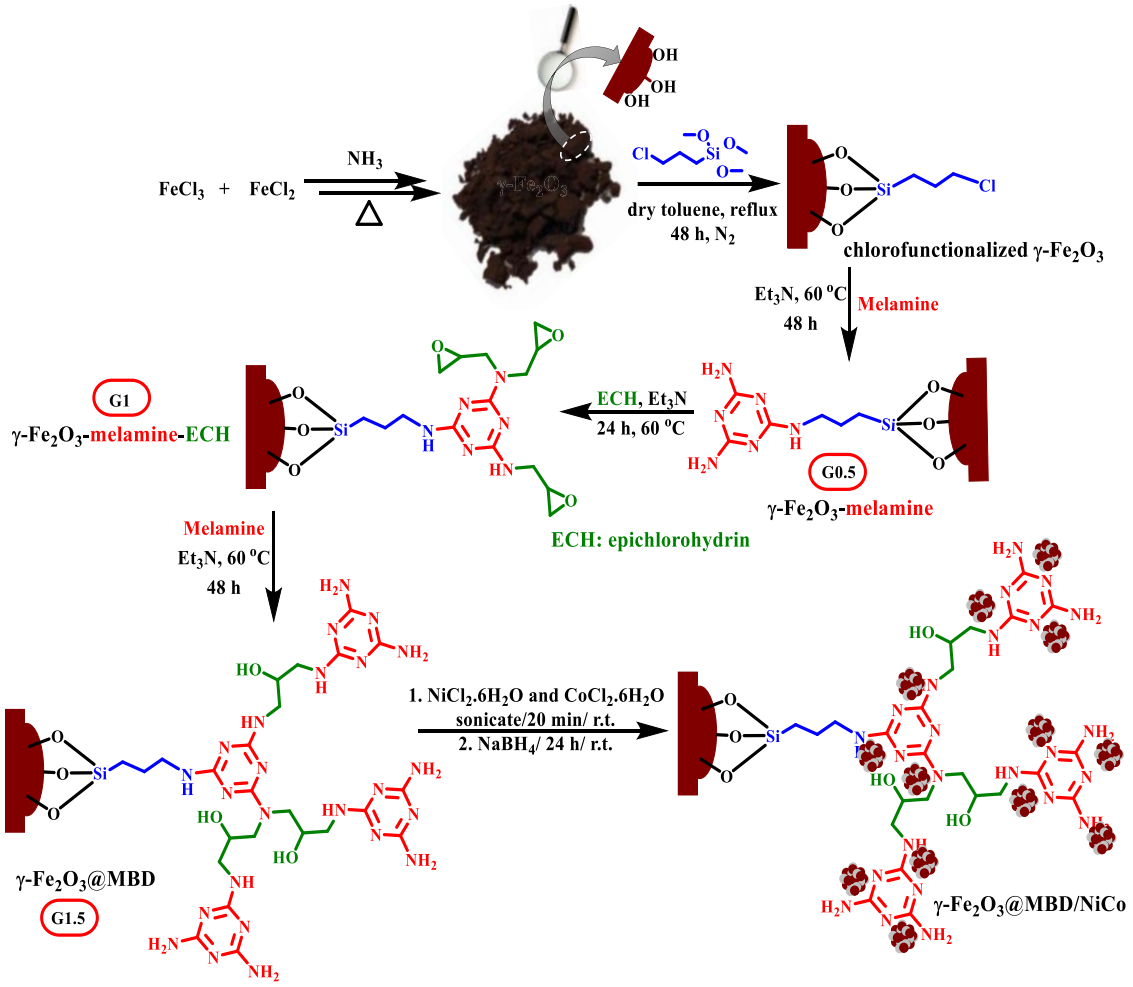

with melamine led to the 1.5 generation of dendrimer–magnetite nanoparticles (γ-Fe_2O_3@MBD, G1.5). The final step was the cross-linking of metal complexes in the inner cavity of γ-Fe_2O_3@MBD, followed by reduction with $NaBH_4$ as a reducing agent. Three types of γ-Fe_2O_3@MBD/NiCo as catalysts were synthesized by initial mixing of different proportions of nickel and cobalt metals (1:1, 1:2, and 2:1) (Table 1, entries 3–5), and two catalysts were prepared with single metals (Table 1, entries 1 and 2). Nickel and cobalt contents of produced γ-Fe_2O_3-MBD/NiCo were measured by inductively coupled plasma (ICP) analysis (Table 1).

Fourier transform infrared (FT-IR) spectra of chlorofunctionalized γ-Fe_2O_3, γ-Fe_2O_3-melamine, γ-Fe_2O_3-melamine-ECH, γ-Fe_2O_3@MBD, and γ-Fe_2O_3@MBD/$NiCo_{1.73}$ are shown in Figure 1. They displayed typical bands at about 564–637, 1035, and 3436 cm^{-1} ascribed to Fe–O, Si–O, and O–H bonds, respectively. Peaks at 1652, 1551, and 813 cm^{-1} in the FT-IR spectra of γ-Fe_2O_3-melamine, γ-Fe_2O_3-melamine-ECH, and γ-Fe_2O_3@MBD were related to the C=N stretching and N–H bending vibrations of melamine.[21] Distinctive bands at around 3470 and 3414 cm^{-1} in the FT-IR spectra of γ-Fe_2O_3-melamine (Figure 1b), γ-Fe_2O_3@MBD (Figure 1d), and γ-Fe_2O_3@MBD/$NiCo_{1.73}$ (Figure 1e) were ascribed to the N–H stretching vibration. In the FT-IR spectrum of γ-Fe_2O_3-melamine-ECH (Figure 1c), the stretching vibration band of N–H of primary amine disappeared and new broad peaks at 3472 and 3375 cm^{-1} appeared, which were related to the vibration of N–H and O–H functional groups. These observations evidenced the effective reaction of melamine with epichlorohydrin. A minor shift and differences in the intensity of the stretching vibration bands of N–H and C=N in triazine in the FT-IR spectrum of γ-Fe_2O_3@MBD/$NiCo_{1.73}$ (Figure 1e) can indicate the metallic element and nitrogen atom interactions.

The X-ray diffraction (XRD) patterns of γ-Fe_2O_3, γ-Fe_2O_3@MBD, γ-Fe_2O_3@MBD/Co, γ-Fe_2O_3@MBD/Ni, Fe_2O_3@MBD/$NiCo_{0.39}$, Fe_2O_3@MBD/$NiCo_{0.89}$, and γ-Fe_2O_3@MBD/$NiCo_{1.73}$ are presented in Figure S1. Peaks at 2θ = 30.2, 35.6, 43.2, 53.8, 57.1, and 62.9° are related to the (220), (311), (400), (422), (440), and (511) reflections of the cubic maghemite.[22] The presence of these peaks in the XRD patterns of the modified

Table 1. Amounts of Ni and Co Supported on γ-Fe_2O_3@MBD

entry	catalyst	amount of Ni (mmol·g^{-1})[d]	amount of Co (mmol·g^{-1})[d]	Co/Ni
1	γ-Fe_2O_3@MBD/Ni	6.15	0	
2	γ-Fe_2O_3@MBD/Co	0	6.86	
3[a]	γ-Fe_2O_3@MBD/$NiCo_{0.86}$	3.23	2.77	0.86
4[b]	γ-Fe_2O_3@MBD/$NiCo_{1.73}$	1.88	3.26	1.73
5[c]	γ-Fe_2O_3@MBD/$NiCo_{0.39}$	4.01	1.57	0.39

[a]Initial Ni/Co ratio = 1:1. [b]Initial Ni/Co ratio = 1:2. [c]Initial Ni/Co ratio = 2:1. [d]Determined by ICP.

https://doi.org/10.1021/acsomega.3c03414
ACS Omega 2023, 8, 36801–36814

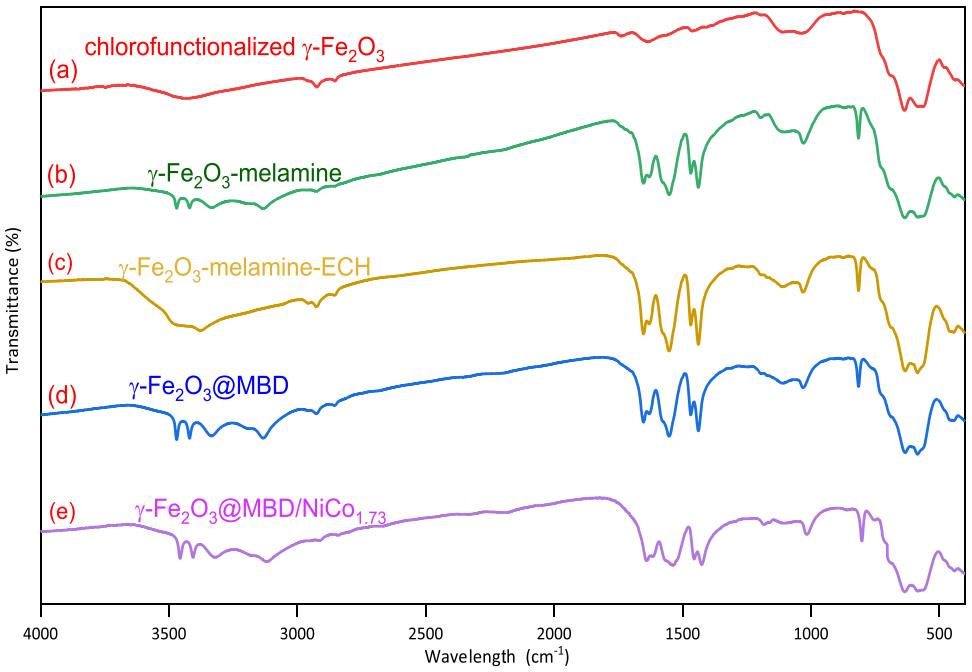

Figure 1. FT-IR spectra of (a) chlorofunctionalized γ-Fe_2O_3, (b) γ-Fe_2O_3-melamine, (c) γ-Fe_2O_3-melamine-ECH, (d) γ-Fe_2O_3@MBD, and (e) γ-Fe_2O_3@MBD/$NiCo_{1.73}$.

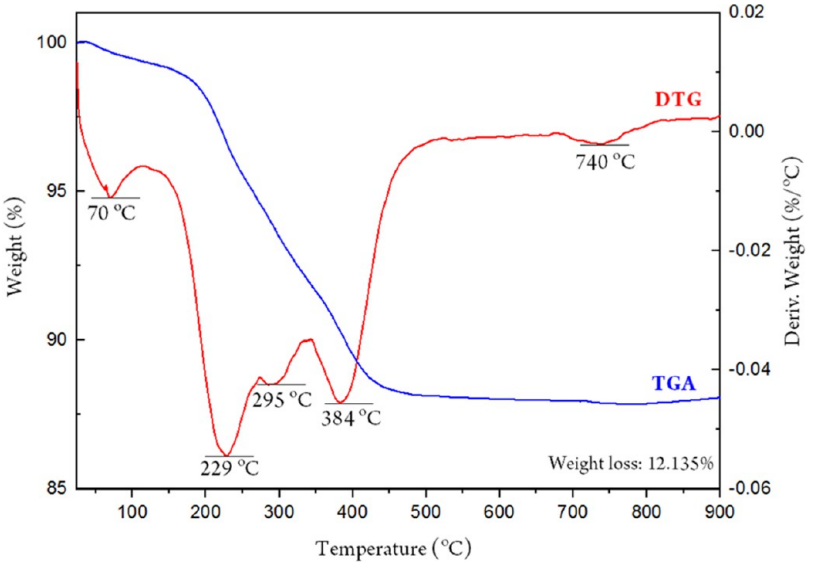

Figure 2. TG-DTG analysis of γ-Fe_2O_3@MBD.

γ-Fe_2O_3 showed that the magnetite structure remained unaffected after coating. Peaks appeared at 11.7 and 25.7° can be ascribed to the successful modification of the γ-Fe_2O_3 surface (Figure S1b−g).[23] In the XRD patterns of γ-Fe_2O_3@MBD/Co and γ-Fe_2O_3@MBD/Ni (Figure S1c,d), the peaks at 47.4 (111), 50.9 (200), and 76.7 (220) are attributed to Co and the peaks at 45.5° (111), 52.0° (200), and 78.3° (220) are assigned to Ni, respectively. The absence of the peaks related to the pure metals (Co and Ni) in the X-ray pattern of Fe_2O_3@MBD/$NiCo_{0.39}$, Fe_2O_3@MBD/$NiCo_{0.89}$, and γ-Fe_2O_3@MBD/$NiCo_{1.73}$ (Figure S1e−g), as well as the observation of peaks at around 40.2, 45.5, 50.5, and 74.5° can be attributed to the production of cobalt−nickel nanoalloys.[24] The intensity of the assigned peaks increased by growing the amount of Co to Ni content, which is an indication of the formation of the NiCo nanoalloy with a more crystalline structure.

Thermogravimetric analysis (TGA) and differential thermal gravity (DTG) of γ-Fe_2O_3@MBD are plotted in Figure 2. Weight loss of 1.18% at ∼50−130 °C corresponded to the loss of physically adsorbed water. The second weight loss was corresponded to the structural decomposition of the linkers in γ-Fe_2O_3@MBD. It was mainly occurred at 229 and 295 °C. At around 345 °C, melamine condensed with the elimination of ammonia, led to the formation of melam, melem, and melon.[25] The temperature range of 384−446 °C can be assigned to the complete decomposition of the melamine residue. The possible phase transformation of γ-Fe_2O_3 occurred at 740 °C.[26] These results justified the immobilization of the melamine-based dendrimers on the magnetic nanoparticles.

https://doi.org/10.1021/acsomega.3c03414
ACS Omega 2023, 8, 36801−36814

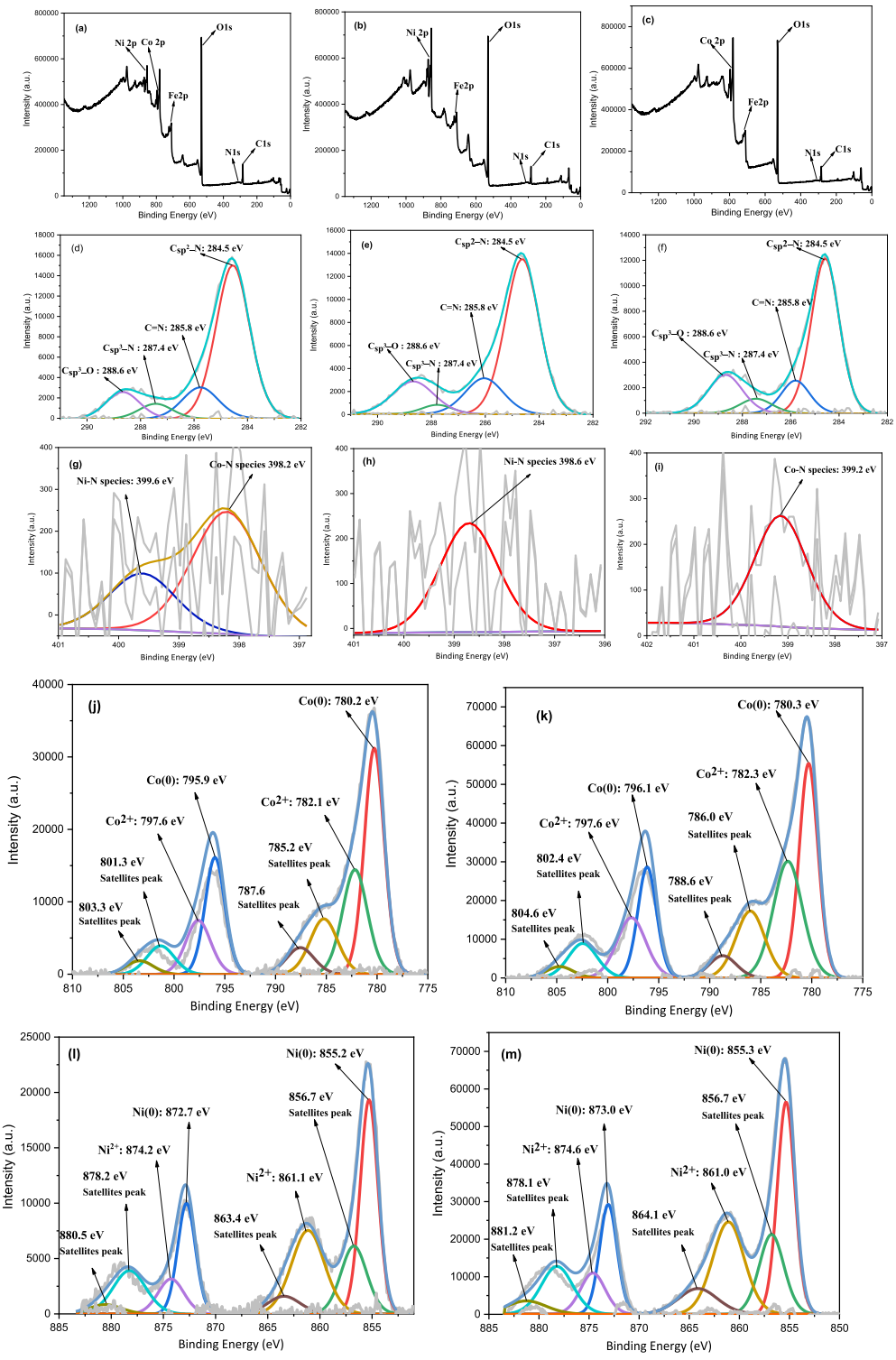

Figure 3. XPS analysis of (a) γ-Fe_2O_3@MBD/$NiCo_{1.73}$, (b) γ-Fe_2O_3@MBD/Ni, (c) γ-Fe_2O_3@MBD/Co, (d) C 1s of γ-Fe_2O_3@MBD/$NiCo_{1.73}$, (e) C 1s of γ-Fe_2O_3@MBD/Ni, (f) C 1s of γ-Fe_2O_3@MBD/Co, (g) N 1s of γ-Fe_2O_3@MBD/$NiCo_{1.73}$, (h) N 1s of γ-Fe_2O_3@MBD/Ni, (i) N 1s of γ-Fe_2O_3@MBD/Co, (j) Co 2p of γ-Fe_2O_3@MBD/$NiCo_{1.73}$, (k) Co 2p of γ-Fe_2O_3@MBD/Co, (l) Ni 2p of γ-Fe_2O_3@MBD/$NiCo_{1.73}$, and (m) Ni 2p of γ-Fe_2O_3@MBD/Ni.

Magnetic properties of γ-Fe_2O_3@MBD/$NiCo_{1.73}$ and γ-Fe_2O_3 were studied using a vibrating sample magnetometer (VSM) at room temperature (Figure S2). Figure S2 shows that the saturation magnetization value of γ-Fe_2O_3@MBD/$NiCo_{1.73}$ is about 67.79 emu·g^{-1}, which is less than that of γ-Fe_2O_3 (80.64 emu·g^{-1}). This drop in the saturation magnetization of γ-Fe_2O_3@MBD/$NiCo_{1.73}$ can be assigned to the melamine-based dendrimer loading on the surface of γ-Fe_2O_3. Hysteresis loop was not observed in the magnetization curves, which indicated the superparamagnetic nature of γ-Fe_2O_3@MBD/$NiCo_{1.73}$.

X-ray photoelectron spectroscopy (XPS) was performed to study the composition and valence states of the elements on the

https://doi.org/10.1021/acsomega.3c03414
ACS Omega 2023, 8, 36801−36814

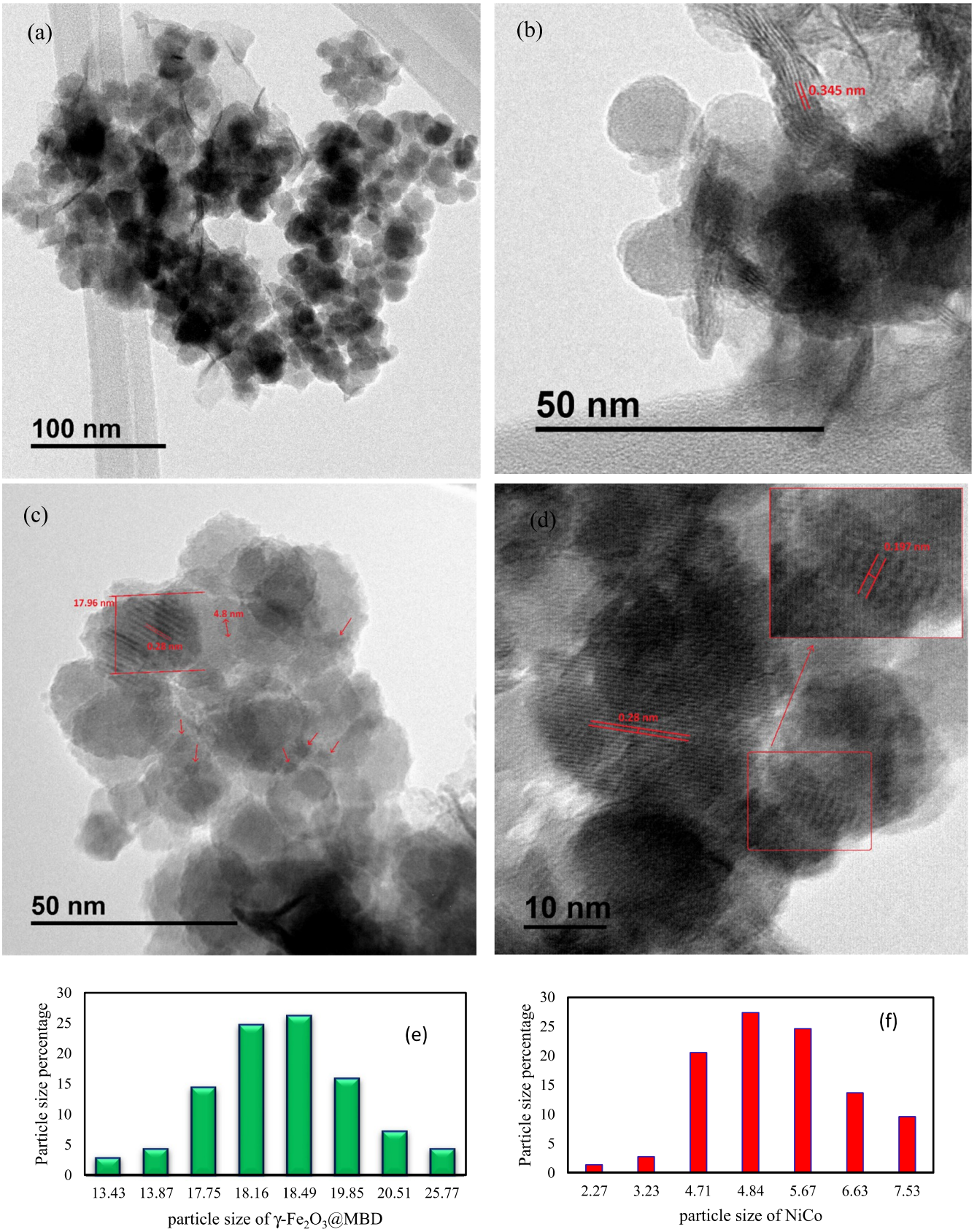

Figure 4. (a–d) TEM images of γ-Fe_2O_3@MBD/$NiCo_{1.73}$. Particle size distribution of (e) γ-Fe_2O_3@MBD and (f) NiCo nanoparticles on the γ-Fe_2O_3@MBD surface.

surface of γ-Fe_2O_3@MBD/$NiCo_{1.73}$, γ-Fe_2O_3@MBD/Ni, and γ-Fe_2O_3@MBD/Co (Figure 3). The XPS spectra revealed the existence of O, C, N, Fe, Ni, and Co in γ-Fe_2O_3@MBD/$NiCo_{1.73}$; O, C, N, Fe, and Ni in γ-Fe_2O_3@MBD/Ni; and Co, C,

https://doi.org/10.1021/acsomega.3c03414
ACS Omega 2023, 8, 36801−36814

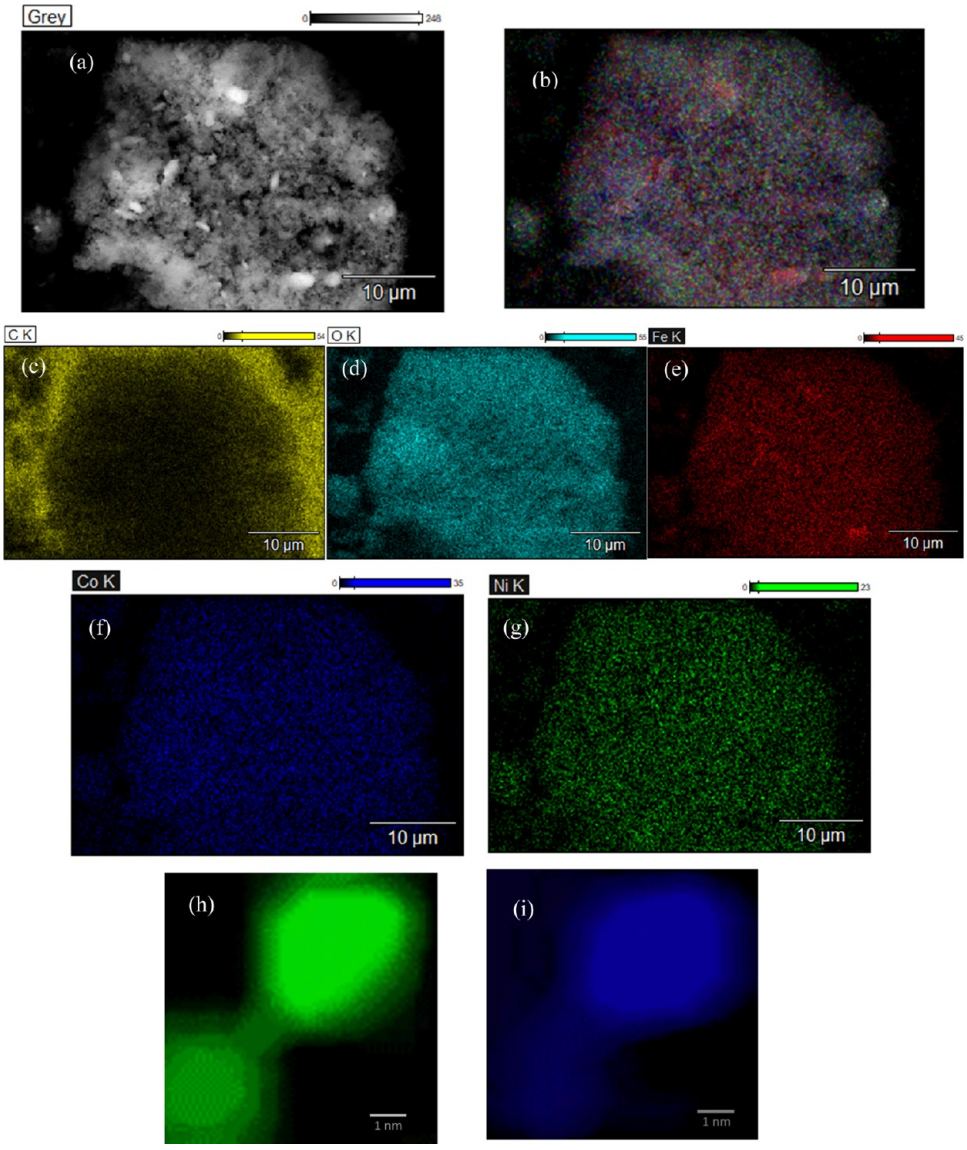

Figure 5. (a) SEM image; EDS mapping images of (b) C, O, Fe, Co, and Ni; (c) C, (d) O, (e) Fe, (f) Co, and (g) Ni in γ-Fe_2O_3@MBD/$NiCo_{1.73}$; and elemental mapping images of (h) Ni and (i) Co with a magnification of 1 nm.

N, Fe, and O in γ-Fe_2O_3@MBD/Co (Figure 3a–c). In the C_{1s} XPS spectra (Figure 3d–f), the peaks at around 284.5, 285.8, 287.4, and 288.6 eV corresponded to C_{sp^2}–N, C═N, C_{sp^3}–N, and C_{sp^3}–O bonds, respectively. In the N_{1s} XPS spectra of Fe_2O_3@MBD/$NiCo_{1.73}$ (Figure 3g), the peaks at 398.2 and 399.6 eV can be assigned to Co–N and Ni–N, respectively.[24c27] The intensity of these two peaks correlated with the molar ratio of Co and Ni but with a small shift in the binding energies compared with those of γ-Fe_2O_3@MBD/Co (Figure 3i) and γ-Fe_2O_3@MBD/Ni (Figure 3h). In the Co_{2p} XPS spectra of γ-Fe_2O_3@MBD/Co (Figure 3k), the binding energies at around 780.3 and 796.1 eV were corresponded to $2p_{3/2}$ and $2p_{1/2}$ of Co(0) species and peaks at around 782.3 and 797.6 eV were related to $2p_{3/2}$ and $2p_{1/2}$ of Co(II) species. In the Ni_{2p} XPS spectra of γ-Fe_2O_3@MBD/Ni (Figure 3m), peaks of Ni(0) species were located at 855.3 and 873.0 eV and the peaks at 861.0 and 874.6 eV were corresponded to Ni(II) species.[28] However, the binding energies of Co(0) and Ni(0) in γ-Fe_2O_3@MBD/$NiCo_{1.73}$ were centered at 780.2 and 795.9 eV and at 855.2 and 872.7 eV, respectively. These shifts can be ascribed to the alloying effect between metallic Co(0) and Ni(0). Furthermore, the XPS analysis revealed that the total ratio of cobalt to nickel is 1.83. The results of the ICP analysis were in line with this and indicate that the surface of NiCo nanoalloys contained more cobalt.

Ni_{2p} and Co_{2p} XPS spectra of γ-Fe_2O_3@MBD/$NiCo_{0.39}$ and γ-Fe_2O_3@MBD/$NiCo_{0.86}$ were compared with those of γ-Fe_2O_3@MBD/$NiCo_{1.73}$, γ-Fe_2O_3@MBD/Ni, and γ-Fe_2O_3@MBD/Co (Figures S3 and S4), and some shifts in the binding energies related to the $2p_{1/2}$ and $2p_{3/2}$ of Co and Ni were observed, which showed the formation of nanoalloys in γ-Fe_2O_3@MBD/$NiCo_{0.39}$ and γ-Fe_2O_3@MBD/$NiCo_{0.86}$. Based on XPS analysis, Co(0)/Co(II) and Ni(0)/Ni(II) ratios in γ-Fe_2O_3@MBD/$NiCo_{1.73}$ are more than those in γ-Fe_2O_3@MBD/$NiCo_{0.39}$ and γ-Fe_2O_3@MBD/$NiCo_{0.86}$ (Table S1).

The surface morphology and size of synthesized γ-Fe_2O_3@MBD/$NiCo_{1.73}$ were investigated by transmission electron microscopy (TEM) analysis (Figure 4). Figure 4a shows that even though these nanoparticles are magnetic, they are dispersed well. This can be due to the presence of a dendrimer with a

https://doi.org/10.1021/acsomega.3c03414
ACS Omega 2023, 8, 36801–36814

lattice fringe of 0.345 nm (Figure 4b) as a suitable coating on the surface of magnetic nanoparticles, which effectively prevents them from agglomeration. The particle size distribution of the magnetic nanoparticles with lattice fringes of 0.28 nm related to the 220-plane[29] is perfectly consistent (Figure 4c,d). The particle sizes of γ-Fe_2O_3 were estimated to be approximately 18 nm (Figure 4e). Spherical NPs with a size of about 4.8 nm were supported on the surface of the magnetic nanoparticles of γ-Fe_2O_3@MBD with uniform size and shape (Figure 4c,f). The existence of nitrogen and oxygen heteroatoms on the surface of γ-Fe_2O_3@MBD can be the cause of this favorable dispersion. The lattice fringe of 0.197 nm (111-plane)[30] in Figure 4d is related to nickel−cobalt nanoparticles with a size of 4.8 nm. The particle size and lattice fringe of the NiCo alloy were considerably smaller than those of Ni (0.621 nm) and Co (0.528 nm) (Figure S5), and this was a proof of the formation of nickel−cobalt nanoalloys (Table S2).

As shown in Figure 5, elemental mapping images of C, O, Fe, Co, and Ni in γ-Fe_2O_3@MBD/$NiCo_{1.73}$ showed the homogeneous distribution of these elements on the surface of the sample. Moreover, energy-dispersive spectrometry (EDS) mapping images of Co and Ni indicated similar distributions (Figure 5f−i), which showed the incorporation of nickel and cobalt into the NiCo nanoalloys. The electronic properties of NiCo nanoparticles were influenced by the incorporation of the individual elements, and so the catalytic performance of the catalyst was increased.

2.2. Reductive Coupling Reaction of Organohalides with Aldehydes Catalyzed by γ-Fe_2O_3@MBD/$NiCo_{1.73}$. At first, to find the optimum reaction conditions, the reaction of benzaldehyde (1 mmol) with bromobenzene (2 mmol) in water catalyzed by γ-Fe_2O_3@MBD/$NiCo_{1.73}$ was selected as the model reaction, and influence of the reductant, temperature, and catalyst amount on the reaction progress was studied (Table 2). The best results were achieved using HCO_2K as the reductant and 0.014 g of γ-Fe_2O_3@MBD/$NiCo_{1.73}$ at 80 °C (Table 2, entry 8).

To evaluate the scope of the reductive coupling reaction, optimal reaction conditions obtained for the formation of secondary alcohol in the model reaction were applied to various aldehydes and organohalides (iodide, bromide, and chloride, Scheme 4). Both aromatic aldehydes containing diverse functional groups and aliphatic aldehydes underwent efficient reductive coupling reactions with organohalides to produce the corresponding secondary alcohols (**1**−**18**, Scheme 4). In all reactions, aryl iodides and bromides showed more activity than aryl chlorides. Aldehyde reduction/dimerization, dehydrohalogenation, or reductive dimerization of aryl halides, the C−N coupling reaction, as well as ketone formation are the most common side products in the reductive coupling reactions. Notably, the formation of the products containing amine groups (**13** and **14**, Scheme 4) demonstrates that aldehydes containing NH functional groups can tolerate the reaction conditions without any C−N coupling formation.

Table 2. Optimization of the Reaction Conditions for Reductive Coupling Reaction between Bromobenzene and Benzaldehyde Catalyzed by γ-Fe_2O_3@MBD/$NiCo_{1.73}$[a]

entry	reductant	temperature (°C)	time (h)	yield (%)
1	HCO_2Na	100	10	85
2	Zn	100	12	55
3	Mn	100	12	60
4	HCO_2NH_4	100	11	85
5	HCO_2H	100	12	50
6	HCO_2K	100	8	90
7		100	24	trace
8	HCO_2K	80	10	95
9	HCO_2K	70	12	85
10[b]	HCO_2K	70	12	80
11[c]	HCO_2K	70	12	85

[a]Reaction conditions: γ-Fe_2O_3@MBD/$NiCo_{1.73}$ [0.014 g, Co (4.56 mol %), Ni (2.63 mol %)], benzaldehyde (1 mmol), bromobenzene (2 mmol), reductant (3 mmol), water (10 mL). [b]γ-Fe_2O_3@MBD/$NiCo_{1.73}$ [0.016 g, Co (5.21 mol %), Ni (3.00 mol %)]. [c]γ-Fe_2O_3@MBD/$NiCo_{1.73}$ [0.012 g, Co (3.90 mol %), Ni (2.30 mol %)].

The recyclability of heterogeneous catalysts is a significant subject from an environmental and practical standpoint. This issue was studied in the model reaction. In an initial experiment, we have found that γ-Fe_2O_3@MBD/$NiCo_{1.73}$ was dispersed in the aqueous layer without any affinity for the organic layer because of the existence of amine and hydroxyl groups in γ-Fe_2O_3@MBD/$NiCo_{1.73}$ (Figure S6a,b). The hydrophilic property of the catalyst helped us to isolate the product completely from the aqueous phase by simple extraction with ethyl acetate (Figure S6b). The catalyst remained in the aqueous phase, separated by an external magnetic field (Figure S6c), and reused successfully for seven consecutive runs (Figure S7). An insignificant decrease in the catalytic activity could be related to the KBr formation during the reaction, which remains in the aqueous phase and might cause the catalyst deactivation. To detect KBr as a side product of the reaction, a solution of $AgNO_3$ was added to the remaining aqueous phase. AgBr as a yellow solid was produced from the reaction of KBr with $AgNO_3$ and was precipitated (Figure S6d). The XRD pattern, FT-IR spectrum, and TEM images of the catalyst recovered after the seventh run indicated that the catalyst remained unaltered (Figure S8). The XPS survey of recycled γ-Fe_2O_3@MBD/$NiCo_{1.73}$ indicated no significant alteration (Figure S9).

The heterogeneity of γ-Fe_2O_3@MBD/$NiCo_{1.73}$ was tested by hot filtration and poisoning tests in the model reaction under the optimized reaction conditions. In order to investigate the hot filtration test, after about 60% of the progress of the reductive coupling reaction of bromobenzene with benzaldehyde, the solid was isolated at 80 °C by a magnetic field and the remaining mixture was stirred for 8 h. Any detection of more transformation indicated that γ-Fe_2O_3@MBD/$NiCo_{1.73}$ acted as a heterogeneous catalyst (Figure S10). In the poisoning test, S_8 (0.05 g) was used as a metal scavenger. As a result, no significant changes were observed during the reaction (Figure S10).

To understand the role of γ-Fe_2O_3@MBD/$NiCo_{1.73}$ in the reductive coupling reaction, the catalytic efficiency of monometallic counterparts, including γ-Fe_2O_3@MBD/Ni and γ-Fe_2O_3@MBD/Co, bimetallic catalyst with different ratios of cobalt and nickel, and a physical mixture of γ-Fe_2O_3@MBD/Ni and γ-Fe_2O_3@MBD/Co were examined in the model reaction using bromobenzene with benzaldehyde and HCO_2K under the optimized reaction conditions (Figure S11). Any byproduct was not formed in the presence of different bimetallic alloys and also γ-Fe_2O_3@MBD/Co. Diphenyl is the only byproduct, which was detected when the reaction was performed in the presence of γ-Fe_2O_3@MBD/Ni and a physical mixture of γ-Fe_2O_3@MBD/Ni and γ-Fe_2O_3@MBD/Co due to more activity of Ni compared with cobalt. However, the catalytic activity of Ni was optimized in the bimetallic nanoalloys, and any byproduct was not formed. The enhanced catalytic activities of bimetallic catalysts with

https://doi.org/10.1021/acsomega.3c03414
ACS Omega 2023, 8, 36801−36814

Scheme 4. Reductive Coupling Reaction of Various Aldehydes and Organohalides Catalyzed by Fe_2O_3@MBD/$NiCo_{1.73}$ in Aqueous Media to Produce Secondary Alcohols[a]

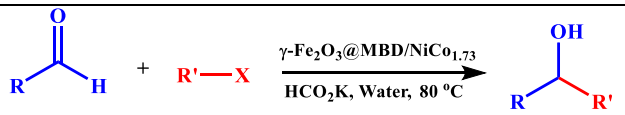

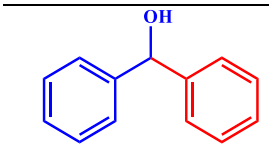

1, 10 h

X = I (80%), Br (95%), Cl (45%)

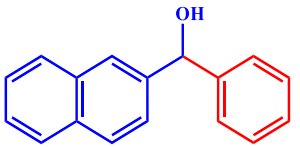

2, 12 h

X = I (70%), Br (85%), Cl (35%)

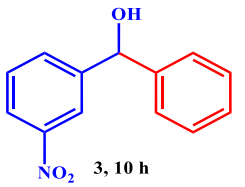

3, 10 h

X = I (85%), Br (90%), Cl (50%)

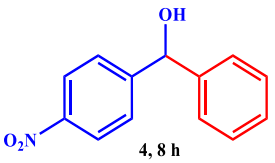

4, 8 h

X = I (88%), Br (92%), Cl (55%)

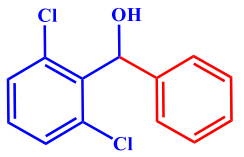

5, 10 h

X = I (85%), Br (80%), Cl (65%)

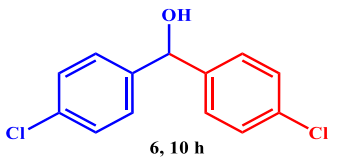

6, 10 h

X = I (90%), Br (87%), Cl (35%)

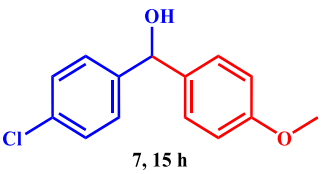

7, 15 h

X = I (80%), Br (77%), Cl (28%)

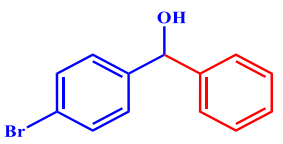

8, 9 h

X = I (85%), Br (80%), Cl (25%)

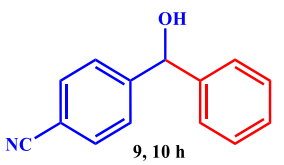

9, 10 h

X = I (88%), Br (85%), Cl (45%)

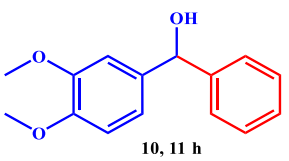

10, 11 h

X = I (70%), Br (75%), Cl (35%)

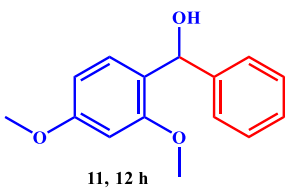

11, 12 h

X = I (75%), Br (72%), Cl (45%)

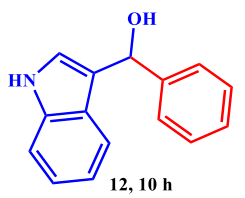

12, 10 h

X = I (80%), Br (82%), Cl (55%)

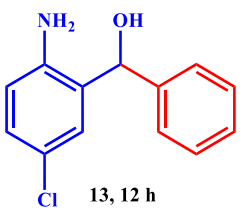

13, 12 h

X = I (80%), Br (88%), Cl (60%)

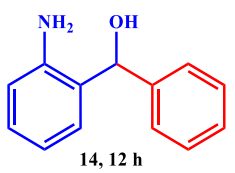

14, 12 h

X = I (75%), Br (85%), Cl (40%)

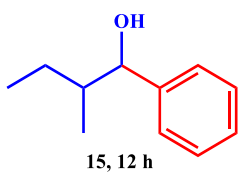

15, 12 h

X = I (75%), Br (70%), Cl (40%)

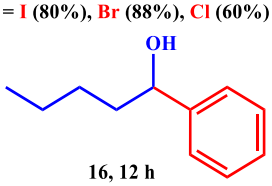

16, 12 h

X = I (70%), Br (72%), Cl (30%)

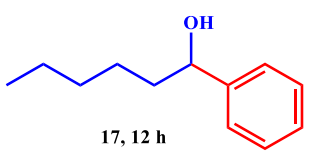

17, 12 h

X = I (65%), Br (68%), Cl (35%)

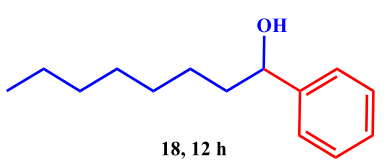

18, 12 h

X = I (70%), Br (65%), Cl (42%)

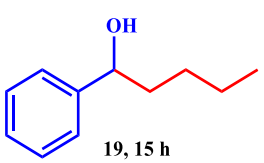

19, 15 h

X = Br (75%)

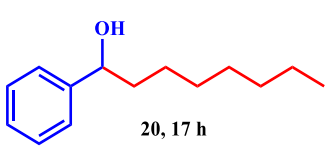

20, 17 h

X = Br (77%)

[a]Reaction conditions: aldehyde (1 mmol), organohalide (2 mmol), HCO_2K (3 mmol), γ-Fe_2O_3@MBD/$NiCo_{1.73}$ [0.014 g, Co (4.56 mol %), Ni (2.63 mol %)], water (10 mL), 80 °C.

https://doi.org/10.1021/acsomega.3c03414
ACS Omega 2023, 8, 36801−36814

Table 3. Catalytic Activity of γ-Fe_2O_3@MBD/$NiCo_{1.73}$ versus the Reported Ni Catalysts for the Reductive Coupling Reaction of Aryl Halides with Aldehydes

entry	catalyst (mol %)	reaction conditions	reductant	X	yield (%)
1[12a]	Ni(bpy[a])Cl_2 (5)	NaI (0.25 equiv), HN^iPr_2 (1 equiv), $(PhO)_2PO_2H$ (1.5 equiv), *n*-hexane, Ar, 95 °C, 7 h	Zn (3 equiv)	I	24−91
2[31]	$Ni(acac)_2$ (5)	toluene, 80 °C, 18 h	2,3,5,6-tetramethyl-1,4-bis(trimethylsilyl)-1,4-diaza-2,5-cyclohexadiene (1.25 equiv)	Br	38−99
3[32]	$NiBr_2$(DME)/L[b] (10)	THF, 70 °C, 24 h	Zn (1.15 equiv)	Br	30−95
4[4a]	$NiBr_2$(diglyme[c])/L[d] (10)	THF, 60 °C, 12−16 h	Zn (1.50 equiv)	I, Br, Cl[e]	29−96
5[33]	$NiBr_2$(dppe[f]) (10)	THF, 75 °C, 24−30 h	Zn (1.3 equiv)	Br	38−91
6[4b]	$NiBr_2$ (diglyme) (5)	$[P(Cy^g)N(ArCF_3)]_2$ (12 mol %), toluene, 75 °C, 16 h	TMP[h] (2 equiv), 1-PhEtOH (3 equiv)	I	18−83
7[34]	$NiBr_2$/L[i] (1.5)	$ZnCl_2$, K_3PO_4, DMSO, photocatalyst[j] (0.2 mol %) 34 W blue LEDs, r.t., 24 h	quinuclidine (30 mol %)	Br	40−83
8[this work]	γ-Fe_2O_3@MBD/$NiCo_{1.73}$ (2.63)	H_2O, 80 °C, 8−15 h	HCO_2K (3 equiv)	I, Br, Cl	25−95

[a]Bipyridine. [b](1*E*,2*E*)-N^1,N^2-Di-*tert*-pentylethane-1,2-diimine. [c]Bis(2-methoxyethyl) ether. [d]5,5′-Dimethyl-2,2′-bipyridine and 4,4′-di-*tert*-butyl-2,2′-bipyridine. [e]100 °C. [f]1,2-Bis(diphenylphosphaneyl)ethane. [g]$C_4H_4CF_3$. [h]2,2,6,6-Tetramethylpiperidine. [i]3,4,7,8-Tetramethyl-1,10-phenanthroline. [j]Ir[2-(2-Fluoro-4-(trifluoromethyl)phenyl)-5-(trifluoromethyl)pyridine]$_2$(4,4′-di-*tert*-butyl-2,2′-bipyridine)PF_6, ($C_{44}H_{34}F_{20}IrN_4P$).

Scheme 5. Sensible Mechanism for the Reductive Coupling Reaction of Aldehydes with Aryl Halides Catalyzed by γ-Fe_2O_3@MBD/$NiCo_{1.73}$

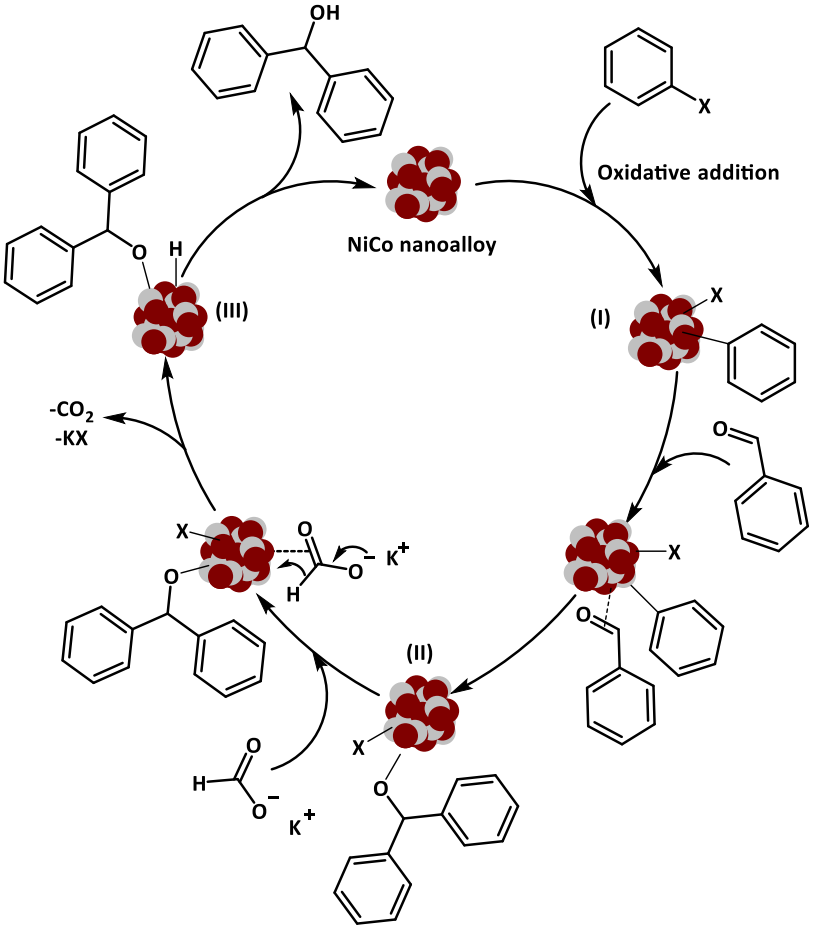

different ratios of cobalt and nickel compared to monometallic counterparts are due to the synergistic effect of both metals in the nanoalloys. Among the bimetallic catalysts, γ-Fe_2O_3@MBD/$NiCo_{1.73}$ provided the corresponding product in higher yield. The presence of Ni and Co in the NiCo nanoalloys in γ-Fe_2O_3@MBD/$NiCo_{1.73}$ with a higher ratio of zero to +2 oxidation state (Table S1) can enhance the electronic effect of the nanoalloys and thus the catalytic efficiency of γ-Fe_2O_3@MBD/$NiCo_{1.73}$. Moreover, as shown in Figure S11, a significant enhancement in the catalytic activity of γ-Fe_2O_3@MBD/$NiCo_{1.73}$ compared to a physical mixture of monometallic counterparts was observed. This observation showed that the synergetic effect needs the presence of the alloy and is not happened just by the presence of both metals in the reaction. Investigation of the model reaction in the presence of γ-Fe_2O_3 or γ-Fe_2O_3@MBD and also in the

https://doi.org/10.1021/acsomega.3c03414
ACS Omega 2023, 8, 36801−36814

absence of the catalyst indicated that the reactions did not proceed at all even after 24 h.

Finally, the catalytic efficiency of γ-Fe_2O_3@MBD/$NiCo_{1.73}$ was compared with that of the reported catalysts containing Ni for the reductive coupling reaction of aryl halides with aldehydes (Table 3). As represented in Table 3, γ-Fe_2O_3@MBD/$NiCo_{1.73}$ exhibited the most effective catalytic activity. The reported methods suffer from drawbacks such as using toxic solvents, high temperature, requiring light irradiation, prolong reaction time, high catalyst loading, and being amenable to limited aryl halides. More importantly, there is no information about the reusability of these reported catalysts in the literature.

Based on the obtained results and previous reports in the literature,[4c] an explanatory mechanism for the reductive coupling reaction of aldehydes with aryl halides was proposed (Scheme 5). In the first step, oxidative addition of aryl halides to the catalyst occurred, and intermediate **I** is formed on the surface of NiCo nanoalloys. Absorption of the aldehyde on the catalyst led to the formation of intermediate **II**. Intermediate **III** was formed in the presence of HCO_2K as a suitable reducing agent. During this process, carbon dioxide was released in the reaction vessel and detected by wet litmus paper (Figure S12). In this process, KBr was also produced, which was detected by the $AgNO_3$ test (Figure S6d). The main problem of reductive coupling reactions is the homocoupling reaction. However, negative shifts in the cobalt and nickel peaks in the XPS spectra of γ-Fe_2O_3@MBD/$NiCo_{1.73}$ (Figure 3j,l) led to reduce the electronic density of NiCo nanoalloys and thus decreased the rate of the oxidative addition step to the catalyst.[35] Therefore, in the next step, the possibility of aldehyde adsorption on the surface of the catalyst was increased. As a result, aldehyde could be added to intermediate **I** rapidly, and the homocoupling product could be avoided.

3. CONCLUSIONS

In this article, bimetallic alloys of NiCo encapsulated in melamine-based dendrimers immobilized on MNPs (γ-Fe_2O_3-MBD@$NiCo_{1.73}$) have been synthesized. The properties and structure of γ-Fe_2O_3-MBD@$NiCo_{1.73}$ were investigated by FT-IR spectroscopy, XRD, XPS, TEM, TGA, VSM, EDS mapping, and ICP analysis. The presence of NiCo nanoalloys was confirmed by XRD and XPS analysis, TEM images, and EDS mapping. Surface coating of magnetic iron oxide nanoparticles with dendrimers brought two practical advantages. First, the surface of the iron oxide nanoparticles was enhanced with nitrogen, which stabilized bimetallic NiCo nanoalloys, and second, the iron oxide nanoparticles were prevented from accumulation and agglomeration, making them stable. TEM analysis showed that these magnetic nanoparticles were well dispersed. We used γ-Fe_2O_3-MBD@$NiCo_{1.73}$ containing NiCo nanoalloys as the first reusable catalyst in the reductive coupling (Barbier−Grignard-type) reaction of organohalides with aldehydes. Using this protocol, various secondary alcohols were obtained in good to high yields without any formation of byproducts such as biaryls as the result of homocoupling reactions, aldehyde reduction/dimerization, or C−N coupling reactions. The synergistic effect of Ni and Co in γ-Fe_2O_3-MBD@$NiCo_{1.73}$ caused high catalytic efficiencies in reductive coupling reactions and selective product formation. Magnetic and hydrophilic properties of the catalyst facilitated the catalyst recyclability for seven consecutive cycles. The reusability of the catalyst, use of water as an environmentally friendly solvent, HCO_2K as a nonmetallic reducing agent, the ease of processing, and the absence of metal additives make this process an excellent choice for the reductive coupling reaction to produce secondary alcohols from aldehydes.

4. EXPERIMENTAL SECTION

4.1. Materials and Methods. Chemicals were acquired from the Merck Chemical Company. The purity of the products and the progress of the reactions were accomplished by thin-layer chromatography (TLC) on silica-gel polygram SILG/UV254 plates. TEM analysis was performed using a TEM microscope (Philips EM 208S). Energy-dispersive spectrometry (EDS) mapping was found using a TSCAN MIRA3. FT-IR spectra were recorded on a Shimadzu Fourier Transform infrared spectrophotometer (FT-IR-8300). Thermal gravimetric analysis (TGA) was performed using a Shimadzu thermogravimetric analyzer (TG-50). XPS analyses were performed using a VG-Microtech Multilab 3000 spectrometer equipped with an Al anode. The deconvolution of the spectra was carried out by using Gaussian−Lorentzian curves. The Ni and Co content on the catalyst was determined by an OPTIMA 7300DV ICP analyzer. Qualitative elemental analysis was determined and analyzed by a CHN elemental analyzer (Thermo Finnigan, FLASH EA 1112 series, Italy).

4.2. Synthesis of γ-Fe_2O_3-Melamine.[17d] A mixture of γ-Fe_2O_3 modified by chlorotriethoxysilane (1.5 g), Et_3N (10 mL), and melamine (1.5 mmol, 0.18 g) was sonicated for 30 min and then stirred under reflux conditions at 60 °C for 48 h. The light-brown precipitate, which was named γ-Fe_2O_3-melamine, was isolated from the mixture by a magnetic field, washed with water (3 × 15 mL) and ethanol (3 × 15 mL), and dried in a vacuum oven at 50 °C. The nitrogen content of the produced γ-Fe_2O_3-melamine was measured by elemental analysis (9.88%). The result indicated that 1.2 mmol of melamine was supported on 1 g of γ-Fe_2O_3-melamine.

4.3. Synthesis of γ-Fe_2O_3-MBD.[17d] A mixture of as-prepared γ-Fe_2O_3-melamine (1 g) and Et_3N (10 mL) was sonicated for 0.5 h at 25 °C. While the mixture was stirred, epichlorohydrin (1 mL) was added dropwise. It was heated to 60 °C and retained for 1 day. After melamine (5 mmol, 0.63 g) was added, the mixture was stirred for 2 days. Then, γ-Fe_2O_3-MBD was separated by a magnetic field, washed with water (3 × 15 mL) and ethanol (3 × 15 mL), and vacuum-dried at 50 °C. The nitrogen content of the produced γ-Fe_2O_3-MBD was measured by elemental analysis (17.5%). The result indicated that 2 mmol of melamine was supported on 1 g of γ-Fe_2O_3-MBD.

4.4. Synthesis of γ-Fe_2O_3-MBD/Ni and γ-Fe_2O_3-MBD/Co. The as-synthesized γ-Fe_2O_3-MBD (0.2 g) was sonicated in H_2O (10 mL) for 20 min. A solution of $NiCl_2{\cdot}6H_2O$ (0.47 g in 10 mL of H_2O) was added, while it was sonicated and the pH was controlled at 8−10 by adding NaOH solution (0.5 M). Then, a fresh solution of $NaBH_4$ (1.0 M, 10 mL) was added to the resulting mixture and stirred for 24 h at 25 °C. The resulting γ-Fe_2O_3-MBD/Ni was isolated from the mixture by a magnetic field, washed with water (3 × 15 mL) and ethanol (3 × 15 mL), and vacuum-dried at 60 °C for 12 h. All of these steps were also done for the synthesis of γ-Fe_2O_3-MBD/Co using $CoCl_2{\cdot}6H_2O$ (0.47 g in 10 mL H_2O). Nickel and cobalt contents of produced γ-Fe_2O_3-MBD/Ni and γ-Fe_2O_3-MBD/Co were measured by ICP analysis. The results showed that 6.15 and 6.86 mmol of Ni and Co were supported on 1 g of γ-Fe_2O_3-MBD/Ni and γ-Fe_2O_3-MBD/Co, respectively (Table 1, entries 1 and 2).

4.5. Synthesis of γ-Fe_2O_3-MBD/NiCo. γ-Fe_2O_3-MBD (0.2 g) and distilled water (10 mL) were added to three flasks (50

https://doi.org/10.1021/acsomega.3c03414
ACS Omega 2023, 8, 36801−36814

mL). Each flask was sonicated for 20 min. $NiCl_2{\cdot}6H_2O/CoCl_2{\cdot}6H_2O$ with molar ratios of 1:1, 2:1, and 1:2 were added to the sonicated samples (Table 1, entries 3−5). The pH of sonicated mixtures was controlled at 8−10 by a NaOH solution (0.5 M). The fresh solutions of $NaBH_4$ (1.0 M, 10 mL) were added to the each reaction mixture and stirred for 24 h at 25 °C. The resulting solids were isolated from the reaction mixtures by a magnetic field, washed with water (3 × 15 mL) and ethanol (3 × 15 mL), and vacuum-dried at 60 °C for 12 h. Nickel and cobalt contents of produced γ-Fe_2O_3-MBD/Ni−Co were measured by ICP analysis. The results are depicted in Table 1, entries 3−5.

4.6. General Procedure for the Reductive Coupling Reaction of Aryl Halides with Aldehydes Catalyzed by γ-Fe_2O_3@MBD/$NiCo_{1.73}$ in Water. γ-Fe_2O_3@MBD/$NiCo_{1.73}$ (0.014 g) was added to a mixture of aldehyde (1 mmol), aryl halide (2 mmol), and HCO_2K (3 mmol) in H_2O (10 mL), followed by increasing the temperature to 80 °C. The progress of the reaction was monitored by TLC. After stirring for appropriate times in accordance with Scheme 4, the reaction was cooled down to room temperature. Ethyl acetate (10 mL) was added, and the organic compound was extracted. $MgSO_4$ was used to dry the combined organic phases. A crude product was obtained by evaporating the organic solvent under vacuum. Purification of the crude product by column chromatography (silica gel) using *n*-hexane/EtOAc (10:3) as the eluent produced the pure product. All of the products were known, and their characterization is reported in the Supporting Information. The catalyst was isolated from aqueous media using an external magnet, washed with water (2 × 15 mL), and reused in the same reaction.

■ ASSOCIATED CONTENT

Supporting Information

The Supporting Information is available free of charge at https://pubs.acs.org/doi/10.1021/acsomega.3c03414.

Copies of NMR spectra, XRD, XPS, TEM, VSM, FT-IR, some figures, and tables (PDF)

■ AUTHOR INFORMATION

Corresponding Author

Sara Sobhani − *Department of Chemistry, College of Sciences, University of Birjand, Birjand 414, Iran;* orcid.org/0000-0002-7764-8847; Email: ssobhani@birjand.ac.ir

Authors

Hamed Zarei − *Department of Chemistry, College of Sciences, University of Birjand, Birjand 414, Iran*

José Miguel Sansano − *Departamento de Química Orgánica, Facultad de Ciencias, Centro de Innovación en Química Avanzada (ORFEOCINQA) and Instituto de Síntesis Orgánica (ISO), Universidad de Alicante, 03080 Alicante, Spain;* orcid.org/0000-0002-5536-2717

Complete contact information is available at: https://pubs.acs.org/10.1021/acsomega.3c03414

Author Contributions

S.S. is the research supervisor and the corresponding author. All of the synthesis reported was performed by H.Z. He also wrote the manuscript draft. J.M.S. performed the XPS, TEM, XRD, EDS mapping, and ICP analysis. All of the authors reviewed the manuscript.

Notes

The authors declare no competing financial interest.

■ ACKNOWLEDGMENTS

Financial support for this project was acknowledged by the Birjand University Research Council. The authors are so grateful to having access to the TEM, XPS, EDS mapping, XRD, and ICP facilities at the University of Alicante.

■ DEDICATION

†Dedicated to Prof. Habib Firouzabadi on the occasion of his 80th birthday.

■ REFERENCES

(1) Peltzer, R. M.; Gauss, J.; Eisenstein, O.; Cascella, M. The Grignard Reaction-Unraveling a Chemical Puzzle. *J. Am. Chem. Soc.* **2020**, *142*, 2984−2994.

(2) Blomberg, C. Synthetic Applications of the Barbier Reaction. In *The Barbier Reaction and Related One-Step Processes*; Blomberg, C., Ed.; Springer: Berlin, 1993; pp 14−74.

(3) (a) Reynolds, J. E., III; Acosta, A. C.; Kang, S.; Li, S.; Lipton, A. S.; Bowden, M. E.; Myllenbeck, N. R.; Schneemann, A.; Leick, N.; Bhandarkar, A.; et al. Teaching an Old Reagent New Tricks: Synthesis, Unusual Reactivity, and Solution Dynamics of Borohydride Grignard Compounds. *Organometallics* **2022**, *41*, 2823−2832. (b) Blomberg, C.; Hartog, F. A. The Barbier Reaction - A One-Step Alternative for Syntheses via Organomagnesium Compounds. *Synthesis* **1977**, *1977*, 18−30. (c) Kavanagh, S. E.; Gilheany, D. G. Harnessing the Power of the Asymmetric Grignard Synthesis of Tertiary Alcohols: Ligand Development and Improved Scope Exemplified by One-Step Gossonorol Synthesis. *Org. Lett.* **2020**, *22*, 8198−8203. (d) Guérinot, A.; Cossy, J. Cobalt-Catalyzed Cross-Couplings between Alkyl Halides and Grignard Reagents. *Acc. Chem. Res.* **2020**, *53*, 1351−1363.

(4) (a) Garcia, K. J.; Gilbert, M. M.; Weix, D. J. Nickel-Catalyzed Addition of Aryl Bromides to Aldehydes To Form Hindered Secondary Alcohols. *J. Am. Chem. Soc.* **2019**, *141*, 1823−1827. (b) Isbrandt, E. S.; Nasim, A.; Zhao, K.; Newman, S. G. Catalytic Aldehyde and Alcohol Arylation Reactions Facilitated by a 1,5-Diaza-3,7-Diphosphacyclooctane Ligand. *J. Am. Chem. Soc.* **2021**, *143*, 14646−14656. (c) Swyka, R. A.; Zhang, W.; Richardson, J.; Ruble, J. C.; Krische, M. J. Rhodium-Catalyzed Aldehyde Arylation via Formate-Mediated Transfer Hydrogenation: Beyond Metallic Reductants in Grignard/Nozaki−Hiyami−Kishi-Type Addition. *J. Am. Chem. Soc.* **2019**, *141*, 1828−1832. (d) Yabushita, K.; Yuasa, A.; Nagao, K.; Ohmiya, H. Asymmetric Catalysis Using Aromatic Aldehydes as Chiral α-Alkoxyalkyl Anions. *J. Am. Chem. Soc.* **2019**, *141*, 113−117. (e) Wang, L.; Wang, L.; Li, M.; Chong, Q.; Meng, F. Cobalt-Catalyzed Diastereo- and Enantioselective Reductive Allyl Additions to Aldehydes with Allylic Alcohol Derivatives via Allyl Radical Intermediates. *J. Am. Chem. Soc.* **2021**, *143*, 12755−12765. (f) Jiang, X.; Jiang, H.; Yang, Q.; Cheng, Y.; Lu, L.-Q.; Tunge, J. A.; Xiao, W.-J. Photoassisted Cobalt-Catalyzed Asymmetric Reductive Grignard-Type Addition of Aryl Iodides. *J. Am. Chem. Soc.* **2022**, *144*, 8347−8354.

(5) Gao, Y.; Hill, D. E.; Hao, W.; McNicholas, B. J.; Vantourout, J. C.; Hadt, R. G.; Reisman, S. E.; Blackmond, D. G.; Baran, P. S. Electrochemical Nozaki−Hiyama−Kishi Coupling: Scope, Applications, and Mechanism. *J. Am. Chem. Soc.* **2021**, *143*, 9478−9488.

(6) Namba, K.; Kishi, Y. New Catalytic Cycle for Couplings of Aldehydes with Organochromium Reagents. *Org. Lett.* **2004**, *6*, 5031−5033.

(7) (a) Takai, K.; Tagashira, M.; Kuroda, T.; Oshima, K.; Utimoto, K.; Nozaki, H. Reactions of alkenylchromium reagents prepared from alkenyl trifluoromethanesulfonates (triflates) with chromium(II) chloride under nickel catalysis. *J. Am. Chem. Soc.* **1986**, *108*, 6048−6050. (b) Fürstner, A. Carbon−Carbon Bond Formations Involving Organochromium(III) Reagents. *Chem. Rev.* **1999**, *99*, 991−1046. (c) Fürstner, A.; Shi, N. Nozaki−Hiyama−Kishi Reactions Catalytic in

Chromium. *J. Am. Chem. Soc.* **1996**, *118*, 12349−12357. (d) Durandetti, M.; Périchon, J.; Nédélec, J.-Y. Nickel- and chromium-catalysed electrochemical coupling of aryl halides with arenecarboxaldehydes. *Tetrahedron Lett.* **1999**, *40*, 9009−9013.

(8) (a) Bower, J. F.; Kim, I. S.; Patman, R. L.; Krische, M. J. Catalytic Carbonyl Addition through Transfer Hydrogenation: A Departure from Preformed Organometallic Reagents. *Angew. Chem., Int. Ed.* **2009**, *48*, 34−46. (b) Santana, C. G.; Krische, M. J. From Hydrogenation to Transfer Hydrogenation to Hydrogen Auto-Transfer in Enantioselective Metal-Catalyzed Carbonyl Reductive Coupling: Past, Present, and Future. *ACS Catal.* **2021**, *11*, 5572−5585. (c) Dubey, Z. J.; Shen, W.; Little, J. A.; Krische, M. J. Dual Ruthenium-Catalyzed Alkene Isomerization−Hydrogen Auto-Transfer Unlocks Skipped Dienes as Pronucleophiles for Enantioselective Alcohol C−H Allylation. *J. Am. Chem. Soc.* **2023**, *145*, 8576−8582, DOI: 10.1021/jacs.3c00934.

(9) (a) Yang, Y.; Sun, Y.; Luo, X. The Relationship between Structure and Catalytic Activity-Stability of Non-Precious Metal-Based Catalysts towards Levulinic Acid Hydrogenation to γ-Valerolactone: A Review. *Energies* **2022**, *15*, No. 8093, DOI: 10.3390/en15218093. (b) Yao, R.-q.; Lang, X.-y.; Jiang, Q. Recent advances of nanoporous metal-based catalyst: synthesis, application and perspectives. *J. Iron Steel Res. Int.* **2019**, *26*, 779−795. (c) Chen, T.; Rodionov, V. O. Controllable Catalysis with Nanoparticles: Bimetallic Alloy Systems and Surface Adsorbates. *ACS Catal.* **2016**, *6*, 4025−4033. (d) Liu, L.; Corma, A. Bimetallic Sites for Catalysis: From Binuclear Metal Sites to Bimetallic Nanoclusters and Nanoparticles. *Chem. Rev.* **2023**, *123*, 4855−4933.

(10) Hannagan, R. T.; Giannakakis, G.; Flytzani-Stephanopoulos, M.; Sykes, E. C. H. Single-Atom Alloy Catalysis. *Chem. Rev.* **2020**, *120*, 12044−12088.

(11) (a) Rajeev, R.; Datta, R.; Varghese, A.; Sudhakar, Y. N.; George, L. Recent advances in bimetallic based nanostructures: Synthesis and electrochemical sensing applications. *Microchem. J.* **2021**, *163*, No. 105910. (b) Singh, A. K.; Xu, Q. Synergistic Catalysis over Bimetallic Alloy Nanoparticles. *ChemCatChem* **2013**, *5*, 652−676.

(12) (a) Ishida, S.; Suzuki, H.; Uchida, S.; Yamaguchi, E.; Itoh, A. Nickel Catalyzed Intermolecular Carbonyl Addition of Aryl Halide. *Eur. J. Org. Chem.* **2019**, *2019*, 7483−7487. (b) Zheng, P.; Xu, W.; Wang, H.; Wang, D.; Wu, X.; Xu, T. Deoxygenative Arylboration of Aldehydes via Copper and Nickel/Photoredox Catalysis. *ACS Catal.* **2022**, *12*, 14926−14933.

(13) Yang, L.; Liu, Z.; Tang, T.; Tang, S.; Li, B.; Wang, B. Ruthenium(II)-Catalyzed Grignard-Type Nucleophilic Addition of $C(sp^2)$−H Bonds to Unactivated Aldehydes. *J. Org. Chem.* **2022**, *87*, 14723−14730.

(14) (a) Shen, K.; Han, X.; Lu, X. Cationic Pd(II)-Catalyzed Reductive Cyclization of Alkyne-Tethered Ketones or Aldehydes Using Ethanol as Hydrogen Source. *Org. Lett.* **2013**, *15*, 1732−1735. (b) Yamamoto, T.; Iizuka, M.; Takenaka, H.; Ohta, T.; Ito, Y. Addition reaction of arylboronic acids to aldehydes and α,β-unsaturated carbonyl compounds catalyzed by conventional palladium complexes in the presence of chloroform. *J. Organomet. Chem.* **2009**, *694*, 1325−1332.

(15) (a) Ambursa, M. M.; Juan, J. C.; Yahaya, Y.; Taufiq-Yap, Y. H.; Lin, Y.-C.; Lee, H. V. A review on catalytic hydrodeoxygenation of lignin to transportation fuels by using nickel-based catalysts. *Renewable Sustainable Energy Rev.* **2021**, *138*, No. 110667. (b) Hatta, A. H.; Jalil, A. A.; Hassan, N. S.; Hamid, M. Y. S.; Nabgan, W.; Alhassan, M.; Bahari, M. B.; Cheng, C. K.; Zein, S. H.; Firmansyah, M. L. A short review on informetric analysis and recent progress on contribution of ceria in Ni-based catalysts for enhanced catalytic CO methanation. *Powder Technol.* **2023**, *417*, No. 118246. (c) Da Costa, P.; Hasrack, G.; Bonnety, J.; Henriques, C. Ni-based catalysts for plasma-assisted CO_2 methanation. *Curr. Opin. Green Sustainable Chem.* **2021**, *32*, No. 100540. (d) De, S.; Zhang, J.; Luque, R.; Yan, N. Ni-based bimetallic heterogeneous catalysts for energy and environmental applications. *Energy Environ. Sci.* **2016**, *9*, 3314−3347. (e) Tsiotsias, A. I.; Charisiou, N. D.; Yentekakis, I. V.; Goula, M. A. Bimetallic Ni-Based Catalysts for CO_2 Methanation: A Review. *Nanomaterials* **2021**, *11*, No. 28, DOI: 10.3390/nano11010028. (f) Bai, J.; Cheng, C.; Liu, Y.; Wang, C.; Liao, Y.; Chen, L.; Ma, L. Selective hydrogenation of levulinic acid to γ-valerolactone on Ni-based catalysts. *Mol. Catal.* **2021**, *516*, No. 112000.

(16) (a) Tian, Z.; Liang, X.; Li, R.; Wang, C.; Liu, J.; Lei, L.; Shu, R.; Chen, Y. Hydrodeoxygenation of guaiacol as a model compound of pyrolysis lignin-oil over NiCo bimetallic catalyst: Reactivity and kinetic study. *Fuel* **2022**, *308*, No. 122034. (b) Zhao, B.; Liu, P.; Li, S.; Shi, H.; Jia, X.; Wang, Q.; Yang, F.; Song, Z.; Guo, C.; Hu, J.; et al. Bimetallic Ni-Co nanoparticles on SiO_2 as robust catalyst for CO methanation: Effect of homogeneity of Ni-Co alloy. *Appl. Catal., B* **2020**, *278*, No. 119307. (c) Gonçalves, V. O. O.; Talon, W. H. S. M.; Kartnaller, V.; Venancio, F.; Cajaiba, J.; Cabioc'h, T.; Clacens, J.-M.; Richard, F. Hydrodeoxygenation of *m*-cresol as a depolymerized lignin probe molecule: Synergistic effect of NiCo supported alloys. *Catal. Today* **2021**, *377*, 135−144. (d) Wang, H.; Li, X.; Lan, X.; Wang, T. Supported ultrafine NiCo bimetallic alloy nanoparticles derived from bimetal−organic frameworks: a highly active catalyst for furfuryl alcohol hydrogenation. *ACS Catal.* **2018**, *8*, 2121−2128. (e) Li, S.; Wang, Y.; Gao, L.; Wu, Y.; Yang, X.; Sheng, P.; Xiao, G. Short channeled Ni-Co/SBA-15 catalysts for highly selective hydrogenation of biomass-derived furfural to tetrahydrofurfuryl alcohol. *Microporous Mesoporous Mater.* **2018**, *262*, 154−165. (f) Li, J.; Wang, Z.; Ma, Y.; Xu, C.; Zhou, S. Synthesis of Mesoporous Silica-Supported NiCo Bimetallic Nanocatalysts and Their Enhanced Catalytic Hydrogenation Performance. *ACS Omega* **2023**, *8*, 12339−12347.

(17) (a) Gao, X.; Tan, Z.; Hidajat, K.; Kawi, S. Highly reactive Ni-Co/SiO_2 bimetallic catalyst via complexation with oleylamine/oleic acid organic pair for dry reforming of methane. *Catal. Today* **2017**, *281*, 250−258. (b) Bharathan, V. A.; Yadukiran, V.; Lazar, A.; Singh, A. P.; Vinod, C. P. Synthesis of Au@Ni bimetallic core shell nanoparticle and nanochains in soyabean oil and their catalytic hydrogenation reactions. *ChemistrySelect* **2016**, *1*, 140−146. (c) Bhunia, K.; Chandra, M.; Khilari, S.; Pradhan, D. Bimetallic PtAu Alloy Nanoparticles-Integrated γ-C_3N_4 Hybrid as an Efficient Photocatalyst for Water-to-Hydrogen Conversion. *ACS Appl. Mater. Interfaces* **2019**, *11*, 478−488. (d) Sobhani, S.; Zarei, H.; Sansano, J. M. A new nanomagnetic Pd-Co bimetallic alloy as catalyst in the Mizoroki−Heck and Buchwald−Hartwig amination reactions in aqueous media. *Sci. Rep.* **2021**, *11*, No. 17025. (e) Kaur, A.; Kaur, G.; Singh, P. P.; Kaushal, S. Supported bimetallic nanoparticles as anode catalysts for direct methanol fuel cells: A review. *Int. J. Hydrogen Energy* **2021**, *46*, 15820−15849. (f) Cheng, J.; Gu, X.; Sheng, X.; Liu, P.; Su, H. Exceptional size-dependent catalytic activity enhancement in the room-temperature hydrogen generation from formic acid over bimetallic nanoparticles supported by porous carbon. *J. Mater. Chem. A* **2016**, *4*, 1887−1894. (g) Waenkaew, P.; Saipanya, S.; Maturost, S.; Themsirimongkon, S.; Somsunan, R.; Promsawan, N. Enhanced catalytic efficiency of bimetallic Pt-Pd on PAMPs-modified graphene oxide for formic acid oxidation. *Int. J. Hydrogen Energy* **2022**, *47*, 16189−16200. (h) Arif, M. A tutorial review on bimetallic nanoparticles loaded in smart organic polymer microgels/hydrogels. *J. Mol. Liq.* **2023**, *375*, No. 121346. (i) Zhao, M.; Wu, Y.; Cao, J.-P. Carbon-Based Material-Supported Palladium Nanocatalysts in Coupling Reactions: Discussion on their Stability and Heterogeneity. *Appl. Organomet. Chem.* **2020**, *34*, No. e5539, DOI: 10.1002/aoc.5539.

(18) Yamamoto, K.; Imaoka, T.; Tanabe, M.; Kambe, T. New Horizon of Nanoparticle and Cluster Catalysis with Dendrimers. *Chem. Rev.* **2020**, *120*, 1397−1437.

(19) Wang, W.; Ruiz, J.; Ornelas, C.; Hamon, J.-R. A Career in Catalysis: Didier Astruc. *ACS Catal.* **2023**, *13*, 1574−1596.

(20) (a) Sobhani, S.; Hosseini Moghadam, H.; Skibsted, J.; Sansano, J. M. A hydrophilic heterogeneous cobalt catalyst for fluoride-free Hiyama, Suzuki, Heck and Hirao cross-coupling reactions in water. *Green Chem.* **2020**, *22*, 1353−1365. (b) Rouzifar, M.; Sobhani, S.; Farrokhi, A.; Sansano, J. M. Cobalt isatin-Schiff-base derivative of MOF as a heterogeneous multifunctional bio-photocatalyst for sunlight-induced tandem air oxidation condensation process. *Sci. Rep.* **2023**, *13*, No. 5115. (c) Chahkamali, F. O.; Sobhani, S.; Sansano, J. M. Water-Dispersible Pd−N-Heterocyclic Carbene Complex Immobilized on Magnetic Nanoparticles as a New Heterogeneous Catalyst for Fluoride-Free Hiyama, Suzuki−Miyaura and Cyanation Reactions in Aqueous

https://doi.org/10.1021/acsomega.3c03414
ACS Omega 2023, 8, 36801−36814

Media. *Catal. Lett.* **2022**, *152*, 2650−2668. (d) Chahkamali, F. O.; Sobhani, S.; Sansano, J. M. A novel base-metal multifunctional catalyst for the synthesis of 2-amino-3-cyano-4H-chromenes by a multi-component tandem oxidation process. *Sci. Rep.* **2022**, *12*, No. 2867. (e) Sobhani, S.; Hosseini Moghadam, H.; Derakhshan, S. R.; Sansano, J. M. Tandem imine formation via auto-hydrogen transfer from alcohols to nitro compounds catalyzed by a nanomagnetically recyclable copper catalyst under solvent-free conditions. *RSC Adv.* **2021**, *11*, 19121−19127. (f) Rouzifar, M.; Sobhani, S.; Farrokhi, A.; Sansano, J. M. Fe-MIL-101 modified by isatin-Schiff-base-Co: a heterogeneous catalyst for C−C, C−O, C−N, and C−P cross coupling reactions. *New J. Chem.* **2021**, *45*, 19963−19976. (g) Khazaee, A.; Jahanshahi, R.; Sobhani, S.; Skibsted, J.; Sansano, J. M. Immobilized piperazine on the surface of graphene oxide as a heterogeneous bifunctional acid−base catalyst for the multicomponent synthesis of 2-amino-3-cyano-4H-chromenes. *Green Chem.* **2020**, *22*, 4604−4616. (h) Jahanshahi, R.; Khazaee, A.; Sobhani, S.; Sansano, J. M. g-C_3N_4/γ-Fe_2O_3/TiO_2/Pd: a new magnetically separable photocatalyst for visible-light-driven fluoride-free Hiyama and Suzuki−Miyaura cross-coupling reactions at room temperature. *New J. Chem.* **2020**, *44*, 11513−11526.

(21) Jiang, L.; Wang, K.; Wu, X.; Zhang, G.; Yin, S. Amorphous Bimetallic Cobalt Nickel Sulfide Cocatalysts for Significantly Boosting Photocatalytic Hydrogen Evolution Performance of Graphitic Carbon Nitride: Efficient Interfacial Charge Transfer. *ACS Appl. Mater. Interfaces* **2019**, *11*, 26898−26908.

(22) Lai, J.; Shafi, K. V. P. M.; Loos, K.; Ulman, A.; Lee, Y.; Vogt, T.; Estournès, C. Doping γ-Fe_2O_3 Nanoparticles with Mn(III) Suppresses the Transition to the α-Fe_2O_3 Structure. *J. Am. Chem. Soc.* **2003**, *125*, 11470−11471.

(23) Liao, Y.; Weber, J.; Faul, C. F. J. Fluorescent Microporous Polyimides Based on Perylene and Triazine for Highly CO_2-Selective Carbon Materials. *Macromolecules* **2015**, *48*, 2064−2073.

(24) (a) Qi, B.; Chang, W.; Xu, Q.; Jiang, L.; An, S.; Chu, J.-F.; Song, Y.-F. Regulating Hollow Carbon Cage Supported NiCo Alloy Nanoparticles for Efficient Electrocatalytic Hydrogen Evolution Reaction. *ACS Appl. Mater. Interfaces* **2023**, *15*, 12078−12087. (b) Wang, H.; Li, X.; Lan, X.; Wang, T. Supported Ultrafine NiCo Bimetallic Alloy Nanoparticles Derived from Bimetal−Organic Frameworks: A Highly Active Catalyst for Furfuryl Alcohol Hydrogenation. *ACS Catal.* **2018**, *8*, 2121−2128. (c) Zhang, X.; Yan, F.; Zhang, S.; Yuan, H.; Zhu, C.; Zhang, X.; Chen, Y. Hollow N-Doped Carbon Polyhedron Containing CoNi Alloy Nanoparticles Embedded within Few-Layer N-Doped Graphene as High-Performance Electromagnetic Wave Absorbing Material. *ACS Appl. Mater. Interfaces* **2018**, *10*, 24920−24929. (d) Chang, Z.; Yu, F.; Liu, Z.; Peng, S.; Guan, M.; Shen, X.; Zhao, S.; Liu, N.; Wu, Y.; Chen, Y. Co−Ni Alloy Encapsulated by N-doped Graphene as a Cathode Catalyst for Rechargeable Hybrid Li−Air Batteries. *ACS Appl. Mater. Interfaces* **2020**, *12*, 4366−4372.

(25) Jo, C.-H.; Jang, Y.-M.; Mun, D.-H.; Yu, C.-J.; Choe, C.-G.; Ri, S.-G. Preparation of acrylic emulsion coating with melamine polyphosphate, pentaerythritol and titanium dioxide for flame retardant cotton/polyethylene terephthalate blend fabrics. *Polym. Degrad. Stab.* **2023**, *214*, No. 110366.

(26) Sakurai, S.; Namai, A.; Hashimoto, K.; Ohkoshi, S.-i. First observation of phase transformation of all four Fe_2O_3 phases ($\gamma \rightarrow \varepsilon \rightarrow \beta \rightarrow \alpha$-phase). *J. Am. Chem. Soc.* **2009**, *131*, 18299−18303.

(27) (a) Chen, H.; Shen, K.; Mao, Q.; Chen, J.; Li, Y. Nanoreactor of MOF-Derived Yolk−Shell Co@C−N: Precisely Controllable Structure and Enhanced Catalytic Activity. *ACS Catal.* **2018**, *8*, 1417−1426. (b) Fu, Y.; Yu, H.-Y.; Jiang, C.; Zhang, T.-H.; Zhan, R.; Li, X.; Li, J.-F.; Tian, J.-H.; Yang, R. NiCo Alloy Nanoparticles Decorated on N-Doped Carbon Nanofibers as Highly Active and Durable Oxygen Electrocatalyst. *Adv. Funct. Mater.* **2018**, *28*, No. 1705094.

(28) (a) Lu, C.; Wu, E.; Li, C.; Dou, W.; Lian, Y.; Liang, Y.; Xiang, X.; Wang, H. CoNi bimetallic alloy cocatalyst-modified γ-C_3N_4 nanosheets for efficient photocatalytic hydrogen production. *J. Phys. Chem. Solids* **2021**, *158*, No. 110228. (b) Hu, S.; Zhou, Y.; He, M.; Liao, Q.; Yang, H.; Li, H.; Xu, R.; Ding, Q. Hollow Ni-Co layered double hydroxides-derived NiCo-alloy@γ-C_3N_4 microtubule with high-performance microwave absorption. *Mater. Lett.* **2018**, *231*, 171−174. (c) Cheng, M.; Wen, M.; Zhou, S.; Wu, Q.; Sun, B. Solvothermal Synthesis of NiCo Alloy Icosahedral Nanocrystals. *Inorg. Chem.* **2012**, *51*, 1495−1500.

(29) (a) Cao, D.; Li, H.; Pan, L.; Li, J.; Wang, X.; Jing, P.; Cheng, X.; Wang, W.; Wang, J.; Liu, Q. High saturation magnetization of γ-Fe_2O_3 nano-particles by a facile one-step synthesis approach. *Sci. Rep.* **2016**, *6*, No. 32360. (b) Li, S.-S.; Li, W.-J.; Jiang, T.-J.; Liu, Z.-G.; Chen, X.; Cong, H.-P.; Liu, J.-H.; Huang, Y.-Y.; Li, L.-N.; Huang, X.-J. Iron Oxide with Different Crystal Phases (α- and γ-Fe_2O_3) in Electroanalysis and Ultrasensitive and Selective Detection of Lead(II): An Advancing Approach Using XPS and EXAFS. *Anal. Chem.* **2016**, *88*, 906−914.

(30) Wu, Z.; Yang, B.; Miao, S.; Liu, W.; Xie, J.; Lee, S.; Pellin, M. J.; Xiao, D.; Su, D.; Ma, D. Lattice Strained Ni-Co alloy as a High-Performance Catalyst for Catalytic Dry Reforming of Methane. *ACS Catal.* **2019**, *9*, 2693−2700.

(31) Yurino, T.; Ueda, Y.; Shimizu, Y.; Tanaka, S.; Nishiyama, H.; Tsurugi, H.; Sato, K.; Mashima, K. Salt-Free Reduction of Nonprecious Transition-Metal Compounds: Generation of Amorphous Ni Nanoparticles for Catalytic C−C Bond Formation. *Angew. Chem.* **2015**, *127*, 14645−14649.

(32) Asachenko, A. F.; Valaeva, V.; Kudakina, V.; Uborsky, D.; Izmer, V.; Kononovich, D.; Voskoboynikov, A. Coupling of aromatic aldehydes with aryl halides in the presence of nickel catalysts with diazabutadiene ligands. *Russ. Chem. Bull.* **2016**, *65*, 456−463.

(33) Majumdar, K. K.; Cheng, C.-H. Ni(II)/Zn-Mediated chemoselective arylation of aromatic aldehydes: facile synthesis of diaryl carbinols. *Org. Lett.* **2000**, *2*, 2295−2298.

(34) Twilton, J.; Christensen, M.; DiRocco, D. A.; Ruck, R. T.; Davies, I. W.; MacMillan, D. W. C. Selective Hydrogen Atom Abstraction through Induced Bond Polarization: Direct α-Arylation of Alcohols through Photoredox, HAT, and Nickel Catalysis. *Angew. Chem., Int. Ed.* **2018**, *57*, 5369−5373.

(35) (a) Kumar, A.; Bui, V. Q.; Lee, J.; Wang, L.; Jadhav, A. R.; Liu, X.; Shao, X.; Liu, Y.; Yu, J.; Hwang, Y.; et al. Moving beyond bimetallic-alloy to single-atom dimer atomic-interface for all-pH hydrogen evolution. *Nat. Commun.* **2021**, *12*, No. 6766. (b) He, X.; Zhang, M.; Jin, Z.; Zheng, J.; Xu, J.; Yin, X.-B. Highly active CoNi nanoparticles confined in N-doped carbon microtubes for efficient catalytic performance. *Dalton Trans.* **2022**, *51*, 16681−16687.

https://doi.org/10.1021/acsomega.3c03414
ACS Omega 2023, 8, 36801−36814